Received: 20 April 2020 | Revised: 29 July 2020 | Accepted: 23 August 2020

DOI: 10.1002/aic.17044

TRANSPORT PHENOMENA AND FLUID MECHANICS

AIChE JOURNAL

# POD analysis of oscillating grid turbulence in water and shear thinning polymer solution

Tom Lacassagne | Serge Simoëns | Mahmoud EL Hajem | Jean-Yves Champagne

INSA de Lyon, Ecole Centrale de Lyon, Univ Lyon, Villeurbanne Cedex, France

**Correspondence**
Tom Lacassagne, Univ Lyon, INSA de Lyon, Ecole Centrale de Lyon, Université Lyon 1, CNRS, LMFA UMR 5509, 69621 Villeurbanne Cedex, France.
Email: tom.lacassagne@gmail.com

**Present address**
Tom Lacassagne, Department of Mechanical Engineering, University College London, London, UK

## Abstract

Oscillating grids are frequently used with water and Newtonian fluids to generate controlled turbulence and mixing. Yet, their use with shear thinning fluids still requires experimental characterization. Proper orthogonal decomposition (POD) is applied to PIV measurements of the flow generated by an oscillating grid in water and a shear thinning dilute polymer solution (DPS) of xanthan gum. The aims are to investigate the ability of POD to isolate periodic flow structures, and to use it to describe the effects of the shear thinning property. A dominance of the low order POD modes is evidenced in DPS. The methods applied in blade stirred tanks to identify oscillatory motion fail here. However, a strong mode coupling in the grid swept region is observed, determined by the working fluid and by an underlying chaotic nature of the flow. Possibilities of reconstructing turbulence properties using high order modes are discussed.

**KEYWORDS**

oscillating grid turbulence, PIV, POD, shear-thinning

## 1 | INTRODUCTION AND BACKGROUND

Improving the understanding of the flow dynamics of non-Newtonian fluids is a current goal for many industrial and environmental applications. In particular, turbulence in non-Newtonian liquids occurs in several industrial applications for the food or pharmaceutical industries.[1,3] For example, bacteria fermentation for the production of vaccines requires the stirring of liquid media with a rheology transitioning from a low viscosity Newtonian behavior to a high viscosity, shear thinning and viscoelastic behavior.[4,5] The level of understanding has not reached that of turbulence in Newtonian fluid yet. This is mostly because of flow interactions with suspended matter giving the fluid its non-Newtonian properties are multiple and complex, and strongly depend on the microscopic nature and properties of this suspended matter. Nevertheless, it is of great importance to improve the understanding of turbulence in non-Newtonian media, since it influences other physical phenomena present in such industrial processes such as passive or reactive scalar mixing, cells growth, or multi-phase mass transfers.

The best way to achieve this, is through fundamental approaches, such as laboratory experiments or numerical simulations. In both type of studies, the situation is often simplified, in terms of geometry and mean flow features, compared to real life conditions, so that the focus can be made on turbulence alone, or turbulence interacting with other phenomenon. The three keys to a relevant experimental approach are the use of accurate measurement techniques, good modeling of the real-life fluid's complex rheology, and use of an efficient way to generate controlled turbulence with a less intense as possible mean flow.

Optical techniques such as particle image velocimetry (PIV), are good candidates to fulfill the first condition. They further provide instantaneous and multi-point measurement of the liquid phase velocity, and allow to estimate many relevant turbulence properties (fluctuating velocities, length scales, time scales ...). They can however only be used in optically transparent solutions, which restricts the set of

fluids that can be studied. Fluids that are not optically transparent need to be modeled, which appeals to the second condition listed above. Model solutions often consist in additives dissolved in Newtonian solvents.

Polymers are widely studied as flow additives because they are at the origin of the non-Newtonian properties of the fluid in many applications, and also because the wide range of existing polymers allows to use them to build model fluids reproducing the behaviors of other non-Newtonian media.[6]A well-known feature of dilute polymer solutions is their elasticity, which comes from the ability of polymer molecules to deform and exchange energy with the base flow,[7-10] and leads to the well-known drag reduction phenomenon, among others.[11,12]But polymer solutions also commonly exhibit shear-thinning behaviours[13,14]: the viscosity of the solution decreases with increasing shear rate. This, for example, is known to have an impact on both oscillatory motions and turbulence in stirred tanks.[5,15]

The last condition is most probably the hardest to meet: generating controlled turbulence, if possible with a negligible mean flow, has been the challenge of many research teams in the last 50 years, in Newtonian fluids to begin with, but also by extension in non-Newtonian fluids. Several experimental designs have been developed to try to achieve turbulence with moderate mean flow, for example arrays of randomly actuated jets,[16] rotating grids,[17] or "washing machine" experiments.[18] In this paper, we focus on one of the most easy to design and commonly used in water: oscillating grid turbulence (OGT). This method consists in making a rigid grid oscillate in a fluid initially at rest. It is usually said that the jets and wakes behind the grid's holes and bars interact to generate turbulence,[19-22] which then diffuses away from the grid. In other words, turbulence comes from the periodic shearing of the fluid by the grid.

Oscillating grid apparatus have been commonly used in experimental fluid mechanics since the seminal works of.[20,21] Numerous applications can be found in the literature, among which the study of interactions between turbulence and solid impermeable boundaries,[23,24] of turbulence and gas–liquid mass transfer at a free surface,[19,25-28] in stratified media,[20,21,29,30] or to study the behavior of bubbles, cells, fibers, and flocculation aggregates suspended in a turbulent liquid phase.[31-35] Oscillating grid stirred tanks are thus tools that allow to generate and study controlled turbulence. They can be used as reference cases to help improve the understanding of conventional (bio)chemical reactors.

The most frequent configuration is that of a grid oscillating vertically in a rectangular section tank with a solid flat bottom and a free surface, and for which the properties of turbulence are studied either above or below the grid swept region, far enough from the liquid/gas or liquid/solid boundary condition. Thompson and Turner[21] studied several types of grids with different mesh sizes $M$ and different bar shapes and thickness $d$. They showed that the best homogeneity and intensity of turbulence was achieved with square section bars and values of a solidity function $f_s(d,M) = \frac{d}{M}\left(2-\frac{d}{M}\right)$ lower than 0.4. These principles have been applied in most oscillating grid experiments ever since.

Moreover, it has been shown by[20,21] and confirmed by a wide number of studies[1,19,25,29,30,36-39] that the Root Mean Square (rms) of turbulent velocity fluctuations decays as one over the distance to the grid average position:

$$< u_z' >_{rms} \sim Z^{-n} \quad (1)$$

with $n = 1$, and

$$< u_x' >_{rms} \sim < u_z' >_{rms} \quad (2)$$

where $u_z'$ and $u_x'$ are respectively the vertical and horizontal turbulent velocity fluctuations, and $<.>_{rms}$ denotes horizontal average (along x, on a $-3M < X < 3M$ span) of ensemble rms values. From an historical perspective, the purpose of such setup has mainly been to generate controlled turbulence away from the grid. As a consequence, until recently,[24,40] no study had focused on oscillatory flows generated by the grid motion in and around its swept region, or on how energy is transferred from the oscillatory forcing to turbulence or mean flow.

The influence of non-Newtonian properties on oscillating grid turbulence has first been studied by Liberzon et al.[41] and Wang et al.[42,43], who addressed questions on turbulence in viscoelastic solutions.[41] observed the propagation velocity of the boundary between turbulent and nonturbulent regions in the grid-stirred tank, at the first instants after the onset of the grid's oscillations. They found that the turbulent/nonturbulent interface moved globally faster in dilute polymer solution than in water[42,43] later used a two oscillating grid system to study the viscoelastic effects of surfactants and dilute polymers on coherent structures of OGT. Using proper orthogonal decomposition (POD), they show that the addition of polymer tends to decrease the small scale effects of turbulence, and that this decrease can not only be attributed to the overall viscosity increase, since it is not associated with a decrease of the turbulent kinetic energy (TKE). Hence the non-Newtonian property of the fluid seems to strongly modify the turbulent spectrum. They show promising results for the use of this method to analyze OGT flow properties in complex fluids such as DPS. It is also worth noting that many studies on fixed (passive) grid turbulence in viscoelastic polymer solutions exist in the literature (see for example, [44,45]), but as the shear forcing is not periodic and thus intrinsically different from the one considered in the present work, they will not be reviewed here in details for the sake of brevity.

The behavior of OGT acting in shear thinning solutions remained unexplored until two of our recent articles.[40,46] It has been showed in[46] that polymer addition tends to promote the mean flow's intensity and structure, and that Equation 1 and 2 remains valid for polymer solutions in the dilute entanglement regime with a concentration dependent $n$ exponent. In Reference 40, the influence of polymer on oscillatory features of the flow around the grid have been described using a phase resolved measurements approach. Despite its suitability for the analysis of periodic motion, this phase averaged method required the collection of important quantity of data and an elaborate data processing.[40,47] It was also only focused on the grid neighborhood only, whereas the non-phase resolved measurements in Reference 46 studied the bulk flow without considering the near grid region.

POD has been recently used in stirred tanks to identify periodic flows induced by blade motions and study their interactions with mean flows and turbulence,[15,48,49] without having to resort to the previous phase averaged measurements. It is also now established as a quick and efficient tool for the study of turbulent flows.[48,50-52]

In this work, POD is thus applied to PIV measurements of OGT in water, and in a shear thinning xanthan gum (XG) solution at a 100 ppm concentration. In that way, we shall connect the results of our two existing studies in terms of both oscillatory flow and turbulence, and investigate several aspects related to OGT in water and dilute polymer solution (DPS) through the following key questions:

- Can POD be used to identify organized motion (local coherent structures or flow periodicity), oscillating velocity fluctuations, and turbulence in an oscillating grid stirred tank?
- If so, how can it help understanding the effects of polymer addition on the flow inside and outside of the grid swept region?

This article comes as a complement to the specific analysis of turbulence properties in the tank,[46] and to the phase resolved analysis of turbulence in the neighborhood of the grid[40] both also presented in Reference 53

## 2 | MATERIAL AND METHODS

### 2.1 | Oscillating grid device

For this study, the grid is placed horizontally in a prismatic tank of inner dimension 277 mm by 277 mm by 550 mm. The walls and the lid of the tank are made of transparent plexiglass to allow flow visualization from various angles. The grid has been made from a plexiglass plate shaped by water jet cutting. It has square section bars of side $d$ = 7 mm and its mesh size is $M$ = 35 mm so that its solidity is $\Xi = \frac{d}{M}\left((2-\frac{d}{M}\right) = 0.36$. This is below the maximum value of $\Xi_{max}$ = 0.4 recommended in Reference 21 for optimal homogeneity of such turbulence. Two of its corners are fixed to piston rods driving its oscillations, and the other two corners are connected to vertical rail rods in order to stiffen the grid during its motion. A periodic translation motion in conferred to the grid by a rotary engine used along with a crankshaft system. Oscillations of the grid are started from a fluid initially at rest, at least 30 min before the beginning of any PIV measurements, to ensure that the flow has reached a stationary state before its velocity is measured. Based on the grid oscillation parameters, a grid Reynolds number $Re_g$ can be defined:[37,54]

$$\mathrm{Re}_g = \frac{\rho f S^2}{\mu} \tag{3}$$

where $\rho$ is the fluid density (equivalent to that of water given the very small mass of polymer added) and $\mu$ the reference fluid viscosity. The grid oscillation frequency is $f$ = 1 Hz and the stroke is $S$ = 45 mm ($S/M$ = 1.28, $S/d$ = 6.42). This gives a $\mathrm{Re}_g$ = 2010 for water at 20°C, and $\mathrm{Re}_g$ = 61 to 1840 for the DPS taking respectively $\mu$ as the zero shear rate or infinite shear rate viscosities. It is stressed that since the viscosity is variable, comparison of Newtonian fluid flow with Non Newtonian fluid flow through the Reynolds number can be difficult. In so we give the $\mathrm{Re}_g$ range accessible by the non Newtonian fluid flow. This at least shows that a large part of the non-Newtonian fluid flow events (high shear rate / low viscosity events) are in the same order of magnitude as the Newtonian ones.

The distance between the grid average position and the bottom of the tank is $H_G$ = 5.5$M$. The tank is filled with fluid up to $H_{tot} = H_G + H_S$ = 460 mm, which corresponds to a total volume of fluid of about 35.5 L and a grid-surface average distance of $H_S \simeq 7M$.

### 2.2 | Properties of polymer solutions

Shear-thinning properties are conferred to the liquid by addition of a minute amount of XG into distilled water. Here a concentration of polymer $C_{XG}$ = 100 ppm is used. This concentration is at the limit between dilute and semi dilute entanglement regime for XG solutions[55]: the non-Newtonian behavior of the flow is dominated by polymer-flow interactions with moderate electrical interactions between polymer chains. The shear thinning behavior of such a solution is modeled by a Carreau–Yasuda equation

$$\frac{\mu-\mu_\infty}{\mu_0-\mu_\infty} = \left(1+\left(t_{CY}\dot{\gamma}\right)^a\right)^{\frac{p-1}{a}} \tag{4}$$

With $\mu_0$ = 32.8 mPa. s the zero shear rate, and $\mu_{\mathrm{inf}}$ = 1.1 mPa. s the infinite shear rate Newtonian plateau. $t_{CY}$ = 1.58 s is a characteristic time scale of the polymer, p-1 = −0.5 is the shear thinning power law exponent, and $a$ = 2 is a parameter accounting for the transition between power law and Newtonian behaviors. The flow curve (viscosity as a function of shear-rate) is provided in supplementary material. Viscoelasticity is checked to be negligible for such a XG concentration (elastic modulus G' and storage modulus G“ have been measured by oscillatory rheological measurements, and G' is much lower than G" for $C_{XG}$ = 100 ppm), as expected.[55]

### 2.3 | PIV measurements

Measurements are performed in the vertical central plane of the grid, in two regions: the close grid region (CG) centered around the grid swept zone (SZ), and the full tank region (FT) between the top of the grid stroke and the bottom of the tank (see Figure 1). PIV acquisition and processing parameters for close grid and full tank studies are indicated in Table 1.

Spurious vectors are removed from PIV fields by applying a threshold of 1.2 on the peak ratio, and replaced using median filtering. It is checked that the proportion of replaced vector is always less than 10% of the total vector number.

The data from CG measurements has been used in Reference 40 for a triple decomposition analysis, and the data from FT measurements has been used in Reference 46 to study the mean flow and

**TABLE 1** Parameters for PIV study of oscillating grid turbulence

| Study | Close grid | Full tank |
|---|---|---|
| $\Delta t$ (ms) | 4 | 18 |
| $f_{acq}$ (Hz) | 10 | 4 |
| Interrogation window size (px-px) | 48–48, 24–24 | 64–64, 32–32 |
| Camera-plane distance (mm) | 300–400 | 800–1,000 |
| f-number | 16 | 16 |
| Spatial resolution (mm) | 3.4 | 2.3 |

*Note:* Spatial resolution denotes the distance between two PIV computed vectors (same along X and Z).

turbulence properties between the grid and the free surface. Note that in the CG region, the grid is visible on particle images. This made it possible in our previous work[40] to know its position within the phase of oscillations, calculate phase dependent velocity statistics, and access the fluctuating components of the velocity field through the Reynolds triple decomposition proposed in Reference 56 Here for CG measurements, in order to improve the quality of PIV measurements around the grid, this later is masked out from images before processing, as described in this previous work.

As mentioned in Reference 40, the smallest Taylor micro-scales of turbulence are found in the water case, for which the viscosity is always the lowest. From the values of integral length-scales and using an homogeneous isotropic turbulence assumption, the Taylor length scales are evaluated to be of 3.17 mm for water, 3.25 mm for a 100 ppm XG solution using a constant viscosity equal to $\mu_\infty$, and 18.17 mm when using $\mu_0$ as the scale viscosity. The spatial resolutions reported in Table 1 are similar to the microscales. This does not allow to evidence energy variations at large wave numbers characteristic of viscoelastic turbulence, and thus limits the analysis to the inertial effects and large scales.

## 2.4 | POD analysis

POD is a linear procedure that decomposes data, here a set of vector fields, into a modal base. It has been used only once to study oscillating grid turbulence[43] in a different setup than the present study (two grids). No conclusion on oscillatory flows in OGT has been drawn from this previous work.

The method applied here for obtaining velocity field decomposition is the snapshot method developed by Sirovich[57] and explained in detail in several articles.[5,49,50] Its principle is briefly recalled here.

The velocity field, is decomposed into a sum of temporal amplitudes $\theta$ (in m/s) and spatial modes $\phi$ (dimensionless):

$$\boldsymbol{U}(x,t) = \sum_{i=1}^{N} \theta^i(t)\boldsymbol{\phi}^i(x) \tag{5}$$

Where N is the number of modes needed to properly reconstruct instantaneous velocity fields, typically of the order of 400–1,000.[5] Instantaneous velocity fields obtained by PIV then have to be reorganized in the form of a sequence of snapshots. To do so, the $(2 \times R \times C) \times N$ snapshot matrix $S_M$ is written as a column-wise assembly of instantaneous velocity components, where $R$ and $C$ are the number of rows and columns of the two-components, two dimensions $R \times C$ vector field.

The POD algorithm then searches for the set of modes that gives the optimal approximation of each instantaneous velocity field in a least square sense, while satisfying the condition that each mode has to be orthogonal to all others. According to Reference [57], this is equivalent to an eigenvalue problem and can be written as

$$\boldsymbol{R\phi} = \lambda\boldsymbol{\phi} \tag{6}$$

Where $\boldsymbol{R} = \frac{1}{N}\boldsymbol{S_M}(\boldsymbol{S_M})^T$ is the two point cross correlation matrix between velocity components, and $\lambda$ (in $m^2/s^2$) is the eigenvalue associated to mode $\phi$. $\lambda$ quantifies the energy content of its associated mode. It is used to sort out the modes from the most to the least energetic.

Once it is done, instantaneous velocity fields can be estimated by reconstruction up to a given number of modes using Equation (5) with an order of summation lower than N. This allows to suppress the small scale of turbulence contribution (high order modes), measurement noise (higher order modes), or even oscillatory motion contributions (coupled and/or oscillatory modes, see the next paragraph). Combination of mode can be used to isolate a relevant set of velocity scales' contribution, assuming that one can give a physical meaning to this collection of modes.

POD has been widely used since the end of the 2000's as an alternative to phase resolved measurements for the identification of trailing vortices and oscillatory flows in stirred tanks.[5,15,48-50,58] Its main advantage is that it requires only a small number of velocity field sampled ($N$ in Equation (5)) and no knowledge of the blade position for each recorded field, while phase resolved measurements require complex timing set-ups and the accumulation of much more instantaneous fields in order to achieve statistical convergence for each blade position. By analogy to this blade stirred tank case, applying POD to the oscillating grid flow should provide information on turbulence and coherent structures in a much quicker and less data-consuming fashion than the phase averaged measurements detailed in,[40] and identify modes that correspond to the oscillatory component of the flow.[5,15,49,59]

This is one of the main interest of applying POD here. In this work, mean velocity is removed from instantaneous fields prior to POD decomposition, hence the mean flow correspond to mode number 0 (i.e., it is not present in the decomposition). A description of the mean flow in similar conditions is available in[46] and its interactions with periodic and turbulence fluctuations is addressed in.[40] Comparing mean flow velocities reported in the two previous works with and POD decomposition in the GN region, the kinetic energy associated to this mean flow is estimated to be an order of magnitude smaller than the kinetic energy attached to the first POD mode for water, and of the same order of magnitude for the polymer case (for which a mean flow enhancement occurs).

Once mean flow and oscillatory motions are identified, higher order modes remaining should correspond to either turbulence or to some peculiar combinations of interactions of modes or waves. The highest order ones then correspond to noise.

The code used here is the one implemented in DaVis 8 software.[60]The average velocity field over 1,000 fields (which are enough for convergence, as demonstrated in[40,46]) is computed and subtracted to instantaneous velocity fields. The POD decomposition is then performed over 1,000 modes using the double precision option. Lower order reconstruction of velocity fields can then be built using a limited number of modes (from 1 to 1,000). If one wants to isolate and describe the behavior of a specific set of intermediate modes, a partial reconstruction from this set only can be deduced from linear combination of two other reconstructions. For example the partial reconstruction using modes 2 and 3 only is computed as the reconstruction up to mode 3 minus the reconstruction based on mode 1 alone. This combination is made possible by the fact that POD is a linear procedure.

POD is applied, as described above, to three regions of interest (ROI) of the flow in the plane of measurement:

- the swept zone (SZ) which is defined as the area covered by the grid motion, and is available in CG measurements
- the grid neighborhood (GN) defined as the upper part of the CG region minus the swept zone (GN=CG-SZ)
- the full tank (FT) ROI defined in Figure 1.

Reference phase resolved measurements are available for the CG (GN and SZ) regions in Reference 40.

## 3 | RESULTS AND DISCUSSION

### 3.1 | POD modes

The two first $\phi$ spatial modes (1 and 2) and a higher number mode (chosen arbitrarily as 60) are represented in Figure 2 for SZ, GN and FT regions, for water and dilute polymer solution. In both liquids, modes 1 and 2 in the SZ region are structures according to the grid design: Six regions of high magnitude corresponding to the six mesh "holes" are visible. Even though the mean velocity field has been subtracted from instantaneous fields prior to POD decomposition, modes 1 and 2 in the FT region show a magnitude field somehow similar to the mean flow intensity displayed in Reference 46 in both water and DPS. Mode 60 is supposed to be associated with turbulence, since it is a high order mode. Indeed, the structures observed are much smaller than for modes 1 and 2, and their magnitude decays when moving away from the grid. Moreover, in all the three regions, the typical size of a high magnitude patch seems smaller in water than in DPS (see for example mode 60, region SZ in water and DPS). Note since the intensity is carried by the temporal mode coefficients, the above color maps should not be used to compare amplitudes from one mode to another, but only between spatial structures of the modes and spatial distribution of $\phi$, as done here.

The above description seems consistent with the general observation that polymer tends to promote larger organized structures and damp the small scales of turbulence and grid turbulence.[43] Turbulence in dilute polymer solutions sees its energy distribution between scales modified. This should be evidenced in the POD decomposition not only by a modification of the high mode structures, but also by an adaptation of the mode by mode energy distribution.

### 3.2 | Energy distribution

Figure 3 shows the eigenvalue spectrum of POD modes, that is to say the magnitude $E_{\lambda_i}$ of each modes divided by the sum of all eigenvalues $\sum_i E_{\lambda_i}$. This ratio quantifies the portion of total kinetic energy included in each mode. It should however be kept in mind that this concerns the measured kinetic energy, which might not be exactly the total kinetic energy actually present in the flow due to experimental limitations (e.g., planar and two-dimensional measurements).

The first modes are representative of large coherent structures (organized motions) and so contain most of the energy. This is especially the case close to the grid where the grid's motion forces the large structures: the first modes have a higher energy share in the SZ region than in the CG region, and in the CG region than in the FT region. The higher order modes are then said to represent turbulence or noise. According to Reference 15,61, the eigenvalue value spectrum of a POD decomposition of a turbulent flow presents a $-11/9$ slope at high modes when plotted on a log–log scale (also plotted on the figure for illustration). The range for which the spectrum follows this slope is here limited. This can be due to two reasons: the relatively low grid Reynolds number which may lead to poor scale separation in all fluids, and the limitations in the spatial resolution of PIV measurements which does not allow to describe the smallest turbulent scales (as mentioned previously). However, it seems that this $-11/9$ slope is reached for lower modes in the FT region, suggesting that such lower modes may there already be related to fine, turbulent scales, as will be confirmed later in the following sections. Note that advanced maximum entropy methods also exist and allow to reconstruct energy density spectra (as a function of wave-number) from POD decomposition and verify their agreement to the conventional $-5/3$ slope in the inertial turbulence range, as described in Reference 62.

In the DPS case, this energetic dominance of the first modes seems to be enhanced: the first eigenvalues share is always higher in the non-Newtonian case than in water, and the eigenvalue spectrum curves for DPS and water cross at a given mode. Lower order modes than this crossover values see their energetic share amplified in DPS whereas higher order modes have their impact decreased. This trend can also be visualized by plotting the cumulative energy as a function of the number of modes, as in Figure 4. It shows that cumulative energy converges towards its total value quicker in DPS than in water, and that for every region of the flow. Fewer modes are necessary to capture most of the kinetic energy in DPS than in water for a given region of the flow. Energy concentrates in the first few modes. This

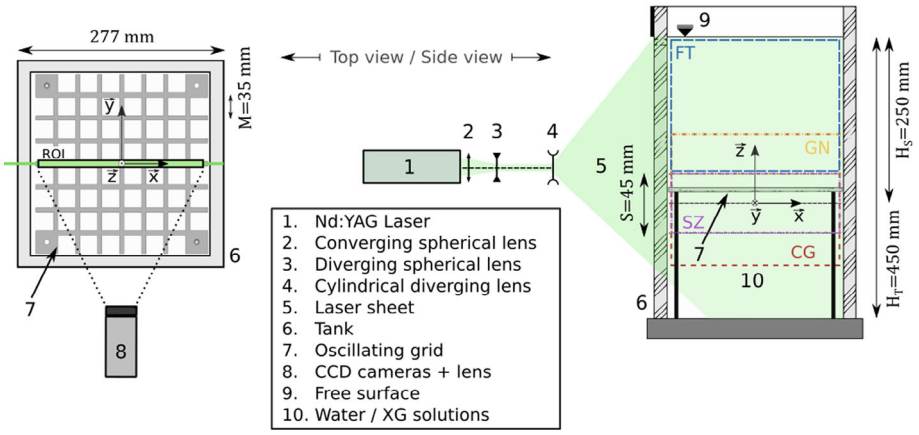


**FIGURE 1** Sketch of the experimental setup and of the regions of study: SZ for Swept Zone, GN for Grid Neighborhood, CG for Close Grid, FT for full tank [Color figure can be viewed at wileyonlinelibrary.com]

has also been evidenced by Reference 61 while studying the drag reduction of polymers in turbulent channel flows, and by Reference 43 in two oscillating grid turbulence of viscoelastic fluids.

A final interesting conclusion can be drawn using eigenvalues. By plotting for FT and SZ regions the eigenvalue spectrum of DPS $E_{\lambda_i}^{DPS}$ normalized by the corresponding eigenvalue spectrum for water $E_{\lambda_i}^{w}$ (Figure 3c)), one shows that for the first modes, the energetic enhancement is more significant for the FT region, which does not include the swept zone of the grid. Indeed, the negative slope of $E_{\lambda_i}^{DPS}/E_{\lambda_i}^{w}$ is decreased for FT as compared to the slopes of SZ. In other words, the steeper decreasing slope with increasing mode number suggests an even stronger low mode (large scales) enhancement in the FT case regardless of the overall value of the dissipation. This observation leads to the conclusion that the enhancement of energy share of the first mode can not only be attributed to organized motions generated by the grid (which are dominant in SZ region), but is also a feature of turbulence in DPS. It can be that small scales of turbulence are damped by the polymer, as previously observed in previous viscoelastic turbulence studies[8,9] and also using POD analysis.[43,61] This translates into a decrease of the high POD modes energy, that are indicators of these small scales. For regions where the grid forcing is not directly felt (FT), the eigenvalue spectrum is intrinsically flatter (see Figure 3) since mean and organized motion caused by the grid are weaker.

In other words, even in Newtonian flows, the energy share is quite balanced between modes in the FT region whereas in the SZ region, energy is more contained in low order modes because of the grid. A damping of small structures is thus more visible in the FT region for which these structures are significant in the flow's energy, than in the SZ region where they are less influential.

All of the above thus to confirm that the shear-thinning behavior and the proximity to the grid promote large scale flow structures (organized or turbulent).

However, one should keep in mind that the DPS viscosity being always higher than that of water, total kinetic energy dissipation is likely higher. In a Newtonian fluid with viscosity analog to that of DPS, and equivalent total dissipation, smaller scales would be larger than in water. This implies that in such a fluid, a given mode number is already associated to larger flow structures (smaller wave numbers) with intrinsically higher kinetic energy content, owing only to differences in viscosity. When normalizing spectra "by mode number", as done in Figure 3c, the effect would thus also be to promote low order modes. It is very difficult to estimate true local dissipation values in shear-thinning fluids, which makes re-scaling of the spectra and normalization "by wave number" challenging. It is thus possible that the slope observed in Figure 3c derives from both differences in "Newtonian" viscous dissipation, and small-scale damping due to the polymer. The latter alone would have potentially led to still decreasing but flatter slopes.

## 3.3 | Identification of organized motion

Let us recall the criterion for the identification of oscillatory modes of the flow in stirred tanks[15,49,59] that we shall use as a starting point for our analysis. Oscillatory components are the results of coupled modes for which:

- two successive eigenvalue values are close to each other in the eigenvalue spectrum (the coupled modes have the same energetic impact).
- the temporal coefficient of each mode i, $\theta_i(t)$, shows a sinusoidal trend when plotted versus time, and its PDF is shaped like that of a sinusoidal function (while that of a turbulent mode approaches a Gaussian shape (as discussed later in Figure 6).
- the scatter plot of two coupled modes arranges in a circle in the $\theta_i$-$\theta_{i+1}$ space.

From the eigenvalue spectrum Figure 3, no couple of successive eigenvalue of equivalent magnitude can easily be extracted, and that even in the SZ region where oscillatory motion is known to be dominant. The second identification criterion yields better results. Indeed, the plot of temporal coefficient intensity as a function of the field index (approximately replacing here time since the measurements are not time resolved) allows to identify a clear sinusoidal behaviors for the first mode in the SZ region for both water and DPS. Since velocity fields are recorded at 10 Hz and the grid frequency is 1 Hz, a periodicity of $P = 10$ in terms of field index is quite logically found for this first,

principal, periodic mode. Modes 2 and 3 also seem to have a periodic behavior, but with a higher frequency (lower $p$, $p$ = 5). In the GN region for water, the sinusoidal behavior of mode 1 disappears and no periodic behavior is observed for the following modes. In the GN region for DPS however, an oscillatory behavior can be observed for mode 1 and 3. Yet, due to the quite low time resolution of measurements, higher flow frequencies cannot be captured by the plots of Figure 5.

The probability density function (PDF) of the values of $\theta^i$ coefficients over 1,000 instantaneous fields for the same set of modes, represented by the histogram plots of Figure 6 completes the information on periodic mode behavior. The PDF of mode 10 always approaches a Gaussian shape, characteristic of random distribution. Coefficients $\theta^1$ for water and DPS in the SZ region have a flat shaped distribution corresponding to their (poorly sampled since not time resolved) sinusoidal like behavior. The PDF of coefficient $\theta^2$ and $\theta^3$ also suggest a nonrandom time distribution of the mode in the SZ region, and so a possible periodicity. All PDFs in the GN region for water are bell-shaped, which is expected from Figure 5. Finally, PDFs of temporal coefficients for modes 1 and 3 in DPS for the GN region also exhibit a quasi-Gaussian shape even if their "time" series plot looks periodic.

To a first approach, all these observations are consistent with the previous remarks based on phase averaged measurements: oscillatory motion can logically be found in the SZ region, but is strongly damped when moving away from the grid, and as a consequence almost invisible in the GN region (for water at least). Polymer has an organizing effect on the flow which tends to promote this oscillatory motion and keep it significant in the vicinity of the grid. However, the distinction between periodic and nonperiodic modes is sometimes arduous due to the poor temporal resolution of our measurements, and also to the periodic behavior of modes that can be less pronounced than in stirred tanks. A conclusion is that evolution and PDF of $\theta$ coefficient alone may not be sufficient to identify clearly periodic modes. A complementary step is thus to check the degree of coupling between modes.

No circular arrangement similar to the one found for oscillatory motion in stirred tank can be observed, for any region, fluid, or pair of successive coefficients ($\theta^i$,$\theta^{i+1}$). This is to some extent not surprising since in the stirred tank case, circular organization of the temporal coefficients is evidenced for a pair of successive modes that exhibit an equivalent magnitude in the eigenvalue spectrum, and no such pair of modes is observed here (Figure 3). In the SZ region for both water and DPS however, the scatter plots of $\theta^1$ versus $\theta^2$ and $\theta^2$ versus $\theta^3$

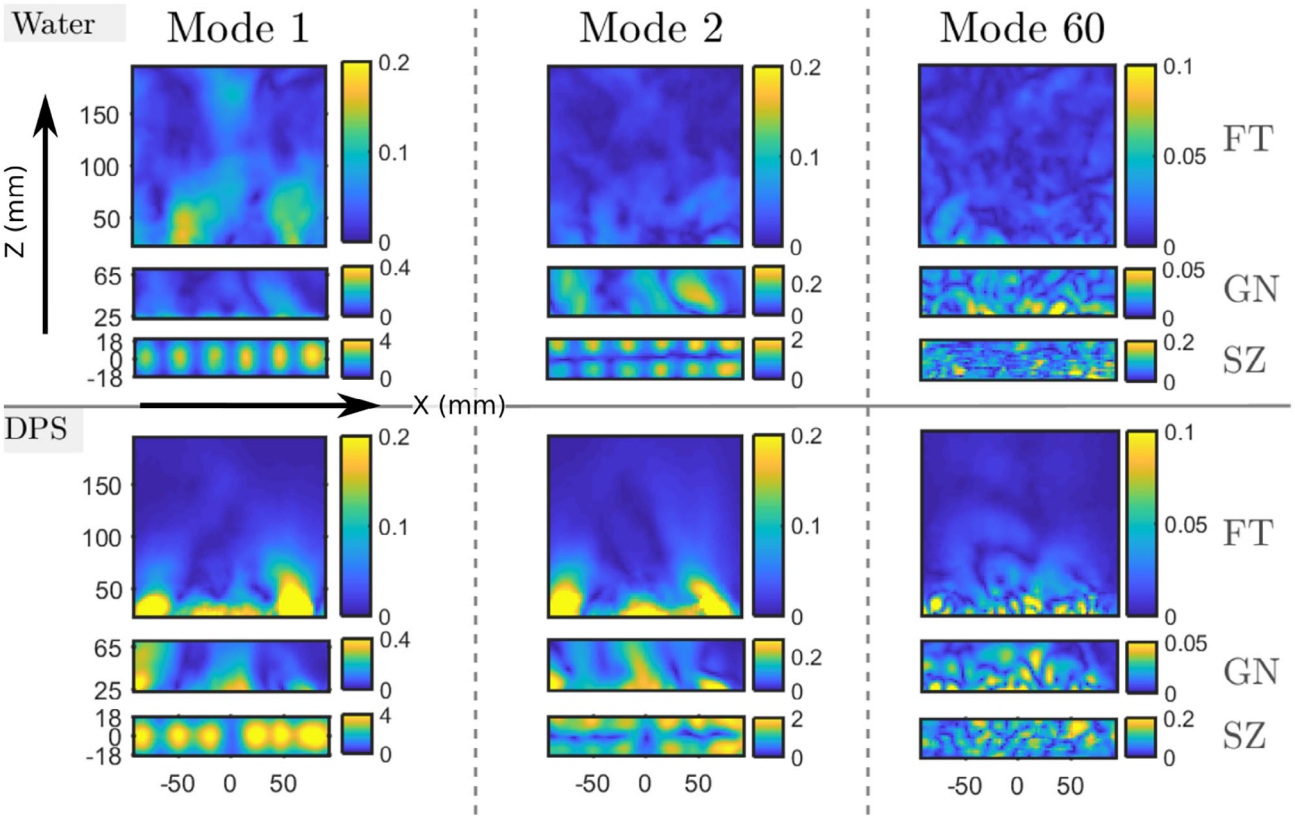


**FIGURE 2** Example of spatial POD modes: modes 1,2 and 60 for regions "Swept Zone" (SZ), "Grid Neighborhood" (GN) and "Full Tank" (FT), in water (top half) and DPS at 100 ppm concentration (bottom half). The color map represents the local non dimensional mode magnitude $\sqrt{(\phi_x^i)^2 + (\phi_z^i)^2}$. Note that these are not reconstructed velocity magnitudes. The velocity intensity is carried by the temporal mode coefficients and modulated by the present maps. The above color maps should not be used to compare one mode amplitude to another, but only between spatial structures of the modes [Color figure can be viewed at wileyonlinelibrary.com]

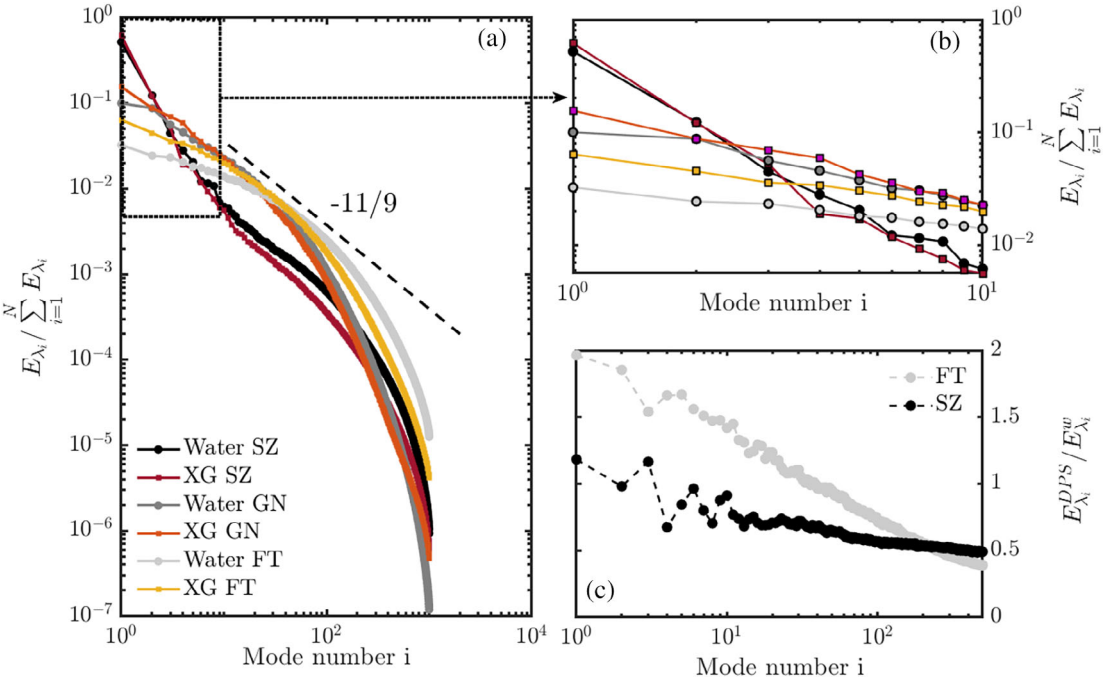


**FIGURE 3** POD eigenvalue spectrum. (a) Full spectrum, (b) zoom on the first 10 modes. (c) POD eigenvalue spectrum of dilute polymer solution normalized by the water spectrum for FT and SZ regions [Color figure can be viewed at wileyonlinelibrary.com]

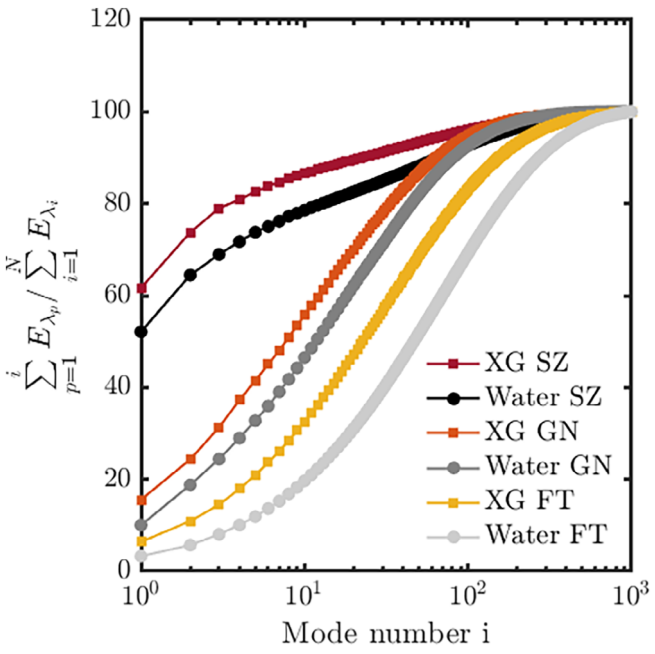


**FIGURE 4** Cumulative energy contained in the POD modes, i axis in log scale [Color figure can be viewed at wileyonlinelibrary.com]

values are not randomly distributed as one would expect for uncoupled modes, but arrange in a more complex characteristic pattern, which can also be seen in three dimension by plotting the 3D scatter plot of $\theta^1$ versus $\theta^2$ versus $\theta^3$ values (see Figure 7). The dispersion around those defined patterns is quite small. The ($\theta^1$,$\theta^2$) pattern has a similar infinity symbol shape for water and DPS, with a variation of the two lobes' sizes and of the crossing point location. ($\theta^2$, $\theta^3$) patterns also include two lobes, but are yet quite different in the two fluids. In the GN region, this settlement disappears.

Infinity shapes, translating into eight-shapes when projected on a 2 modes space, could possibly be related to the frequency of one mode being twice that of the second one (e.g modes 1 and 2 for water, Figures 5 and 7). Not all mode pairs fit this scenario. For example modes 2 and 3 in DPS display a two lobes structure (and not an 8 shaped one), while the frequency of mode 3 is twice that of mode 2 in Figure 5.

In Reference 50, similar patterns of mode coupling are observed in stirred tanks, and used them to evidence a triadic interaction involved in energy transfer between modes. The observation of Figure 7 and the work previously cited still allows to formulate two hypothesis:

- These shapes are a consequence of the strong oscillatory motion observed in the SZ region but not in the GN region, and this motion can not be described by a simple two-mode coupling, but a triadic interaction is likely involved
- The presence of polymer modifies the features of oscillatory motion in the SZ region. This is expressed in POD decomposition by a variation in the coupling between low order modes

The energy transfer between modes likely corresponds to an energy transfer between different types of periodic structures of the flow. In stirred tanks, several types of trailing vortices have been evidenced[49] and exchange energy.[50] The main one is the trailing vortices behind the blades of the impeller. In the oscillating grid system,

we know that the main oscillatory motion is composed of alternating jets and wakes around the grid bars and holes, and that a secondary oscillatory motion exists, such as periodic vortices near the walls. The key difference between the topology of the principal oscillatory structures is that in stirred tanks, the trailing vortices always revolves in the same direction whereas in OGT the direction of the periodic motion changes. For a fluid particle in the region of interest the motion induced by the principal periodic motion will always be null or in a given direction, whereas in the OGT case it can be along different direction of the same axis. Moreover, in the stirred tank case, turbulent structures once generated by the blade evade the swept zone and are left to evolve and dissipate freely in its wake, while in the grid-stirred case, eddies generated by one grid pass almost immediately re-interact with the grid half a period later, making turbulence and periodic structures strongly coupled.

We infer that the triadic coupling comes from the energy transfer between oscillatory component of the flows, some of which have changing directions or signs. The specific shape of these structures in OGT is yet to be explained. It could be in some ways linked to an energy transfer efficiency between modes and consequently between flow structures. An interesting next step would thus be to develop a criterion based on the shape of these patterns to quantify inter modal energy transfer and see its evolution with stirring conditions (Reynolds number, Deborah number ...).

As a last remark, regarding as if subjacent trajectories in the phase space could be induced by such a low order mode coupling, we can notice similarities with chaotic motion figures in laminar flows.[63] Indeed, the temporal amplitude $\theta$ patterns in Figure 7a,c strongly remind the shape of chaotic attractors. This point could be worth investigating in order to explain the patterns' shapes. The following question then arises: may those results indicate an underlying chaotic behaviour in the grid swept zone, possibly issued from a laminar, low grid Reynolds number $Re_g$, chaotic process? A positive answer to the previous question could for example lead to the observation of specific mixing trends in the swept region implied by the subjacent chaotic process, or to further mixing at higher concentration of polymer for which turbulence like traces disappear. Figure 7 could thus be the evidence of a secondary mixing mechanism, possibly chaotic or at least characterized by complex oscillations, efficient near the grid and in low Reynolds number turbulence-free flows.

As one can see, organized motion is difficult to identify using the common criterion for stirred tanks. In other words, POD fails to identify unequivocally local coherent structures, but still provides an information on the global periodicity of the flow through a set of modes. One of the interest of POD is that it makes it possible to reconstruct velocity field using a specific set of modes. With the objective of identifying purely turbulent motion free of any oscillatory component, it is thus easy to remove the oscillatory component from non phase resolved measurements, provided that the modes responsible for oscillatory motion can be identified.

From the above, and as an extension of the existing criterion in blade stirred tanks, we suggest that closed patterns in temporal modes scatter plots could be used as an indicator to unambiguously identify modes involved in oscillatory motion description. Further investigation on multi-modes coupling patterns, in three or more mode dimensions, and how these patterns project in two mode dimension space (Figure 7) is yet still needed.

### 3.4 | POD reconstruction of turbulence properties (FT)

What can still be done in a first approximation is define a threshold mode number for turbulence properties reconstruction. Indeed it is now admitted that oscillatory motion is described by coupling of low order modes, especially in the SZ region. In the GN region, even low order modes are difficult to identify as oscillatory and/or coupled using their temporal amplitude $\theta$ (see Figures 5–7). By setting a limit number of modes considered to be part of the oscillatory motion, one implicitly sets a limit under which modes are considered periodic and nonturbulent, and above which they are considered as turbulent and nonperiodic. It is thus possible to use high order modes only for the reconstruction and estimation of turbulence properties, free of any mean or oscillatory motion, but there is a risk that large scales of turbulence have been artificially removed by suppressing the low order modes. What is proposed here is to check the influence of low order mode removal on the statistical properties of reconstructed velocity fields. Partially-reconstructed fluctuating velocity fields are then calculated by subtracting the reduced order models to the full reconstruction. By this method one gets velocity fields estimated using modes $M_R$ + 1 to 1,000. These are denoted as $M_{R-end}$ POD reconstructions. In the two following paragraphs, reconstruction is performed in the FT region. The turbulent velocity rms profiles along depth, and the power spectra of turbulence reconstructed using different sets of modes are compared.

#### 3.4.1 | Profiles of rms velocity

The rms velocity profiles along the vertical direction are estimated by horizontal averaging over the FT region of the rms velocity fields obtained after POD reconstruction. Vertical profiles of $\left\langle u'_{z,M_R-end}\right\rangle_{rms}$ for water and DPS in the FT region are plotted in Figure 8, and follow power law shaped decay as expected from Equation 1. Profiles for $M_R$ = 1 are for the vertical velocity fluctuations corresponding to the horizontal velocity fluctuations profiles already reported in Reference[46]. The main effect of low order mode removal on reconstructed fields is visible in this figure. It is a decrease of the rms velocities and thus of the TKE. Removing the most energetic modes from reconstruction leads to a decrease in the rms of fluctuating velocity. This is not surprising since the first POD modes are the ones carrying most of the fluctuating kinetic energy. The effect is even more significant in the DPS case where low order modes are associated to a higher energy content. In order to get beyond simple energy removal effects, one may consider the profiles of rms velocity $\left\langle u'_{z,M_R-end}\right\rangle_{rms}$ corrected by the energy loss due to mode removal

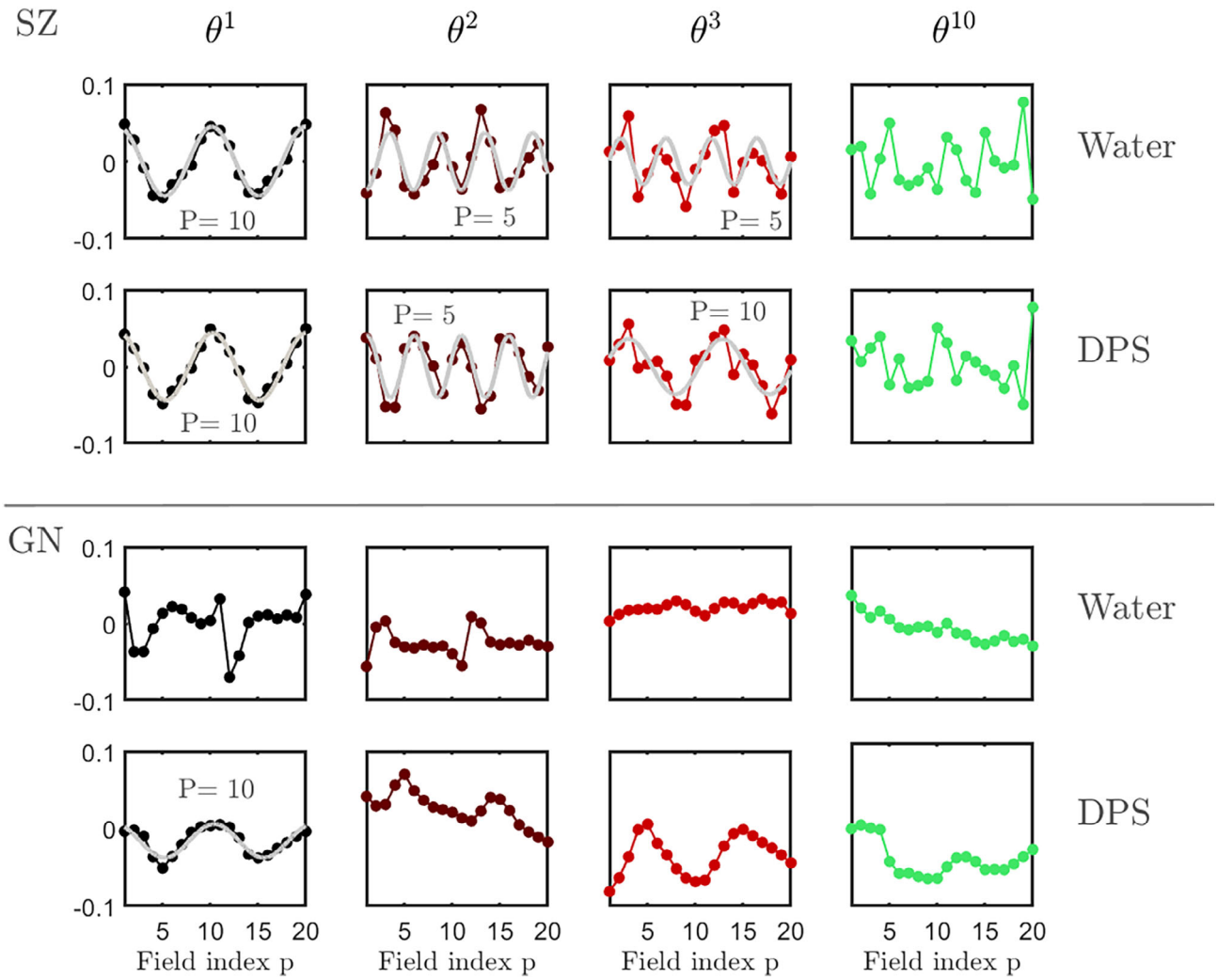


**FIGURE 5** $\theta^j$ coefficients as a function of the instantaneous field index. Modes 1, 2 and 3 are represented as modes for which a periodic behavior can be expected. Mode 10 (chosen arbitrarily among highest mode numbers) is used as a reference for nonperiodic modes. Superimposed light gray lines are best sinusoidal fittings using the full series of snapshots for modes exhibiting a periodic behavior. The period P of each sinusoidal fitting, expressed in field numbers, is indicated in each plots [Color figure can be viewed at wileyonlinelibrary.com]

(Figure 8). Here the chosen scaling is a division by a factor $\sqrt{1-e}$ where $e = \frac{1}{100}\frac{\sum_{p=1}^{M_R} E_{\lambda_p}}{\sum_{i=1}^{N} E_{\lambda_i}}$ is the portion of kinetic energy carried by the removed modes derived from Figure 4. The scaling factor $\sqrt{1-e}$ thus corresponds to a reference velocity built on the total energy carried by the remaining modes. Scaled rms velocity profiles are plotted in Figure 8b,d, and are found to collapse for both water and DPS in a single profile with a well-defined power law region characteristic of oscillating grid turbulence. Removing the first modes before velocity reconstruction does not affect the shape of the rms velocity profiles (the n exponent). It means that the contribution of the first modes to the rms has the same dependency on the grid distance than that of the following modes, that is to say the one depicted by the normalized profile. It either means that the decay law for oscillating velocity fluctuations is the same than the one for turbulent velocity fluctuations, or that the first modes are already significantly representatives of turbulence. Here the most likely conclusion is that in the FT central region, oscillatory motion is nonexistent, or too weak for it to be captured efficiently by POD, so that first modes are already indeed turbulent modes. It is worth noting that for this FT region, no phase-resolved measurement is available, so there is no way to check that this oscillatory motion is truly not present. However phase averaged measurements in the CG region have shown that periodic fluctuations are strongly damped when moving away from the grid, and are very low outside of the SZ region in the central part of the tank.[40] It is thus not surprising that no oscillatory behavior is captured by POD in the FT central region. Applying a similar reconstruction procedure to the SZ region would probably lead to normalized rms profiles highly dependent on the presence or removal of the first POD modes.

### 3.4.2 | Turbulence spectra

In the FT region, 1D power spectra can be computed from the Fourier transform of the cross correlation coefficient of the velocity field. For that purpose, two-point auto-correlation coefficients $R_i^j(M,r_j)$ are

computed for each velocity component $i$, in each direction $j$, with $r_j$ the distance between M and a second point, and $i = x$ or $y$ and $j = x$ or $y$. First evaluated at every location M of the ROI, correlation coefficients are then spatially averaged on M over x and y, and 1D power spectra $P_i^j$ computed by Fourier transform of individual correlation coefficient curves $R_i^j$. This yields power spectrum for the tangential and longitudinal fluctuating velocity components respectively $P_l = 0.5\left(P_x^x + P_y^y\right)$ and $P_t = 0.5\left(P_x^y + P_y^x\right)$. The cumulative power spectrum $P$ is defined as the sum of the last two.[64] It is plotted in Figure 9 for water and DPS using various reconstructions: one including the full set of modes (black dots), some using the first few modes only ($M_0 - M_i$, empty markers), and the complementary reconstructions using the higher order modes only ($M_i - end$, full markers).

From Figure 9, it can be checked that the low order modes are associated to the lower wave numbers k hence to the larger structures of turbulence. Indeed, the empty marker spectra corresponding to reconstructions using only the lower order modes are dominant at low k values but quickly decrease with increasing k. For $k > 2.10^2$ typically, spectra build on higher order modes (full markers) are superimposed with the one reconstructed on the full set of modes. It indicates that at these wave numbers, turbulence can be described by the higher order modes only.

For low wave numbers, fully reconstructed spectra are better matched by the partial reconstructions using high order modes. Yet in the previous paragraph, it was shown that these low order modes are not likely oscillatory or periodic components of the flow. They should thus already correspond to large, random, turbulent structures. This last assumption can be checked by looking at the slopes of the power spectra at low wave numbers in Figure 9. The energy input by the grid occurs at large spatial scales, described by low wave numbers of magnitude between $1/S$ and $1/M$ (dashed/dotted vertical lines) corresponding respectively to one over the amplitude of oscillations and one over the mesh parameter. With increasing wave numbers, the fully reconstructed power spectrum gradually tends to a $-5/3$ slope trend characteristic of the inertial sub-range of turbulence. It is worth noting that the turbulence Reynolds numbers used here are quite low (Taylor based Reynolds number around 30) and it is not surprising that this $-5/3$ slope is not well developed on the measured spectra. Yet an important observation on POD reconstruction can be made: when removing first order modes from the reconstruction, the wave number range in which the slope of

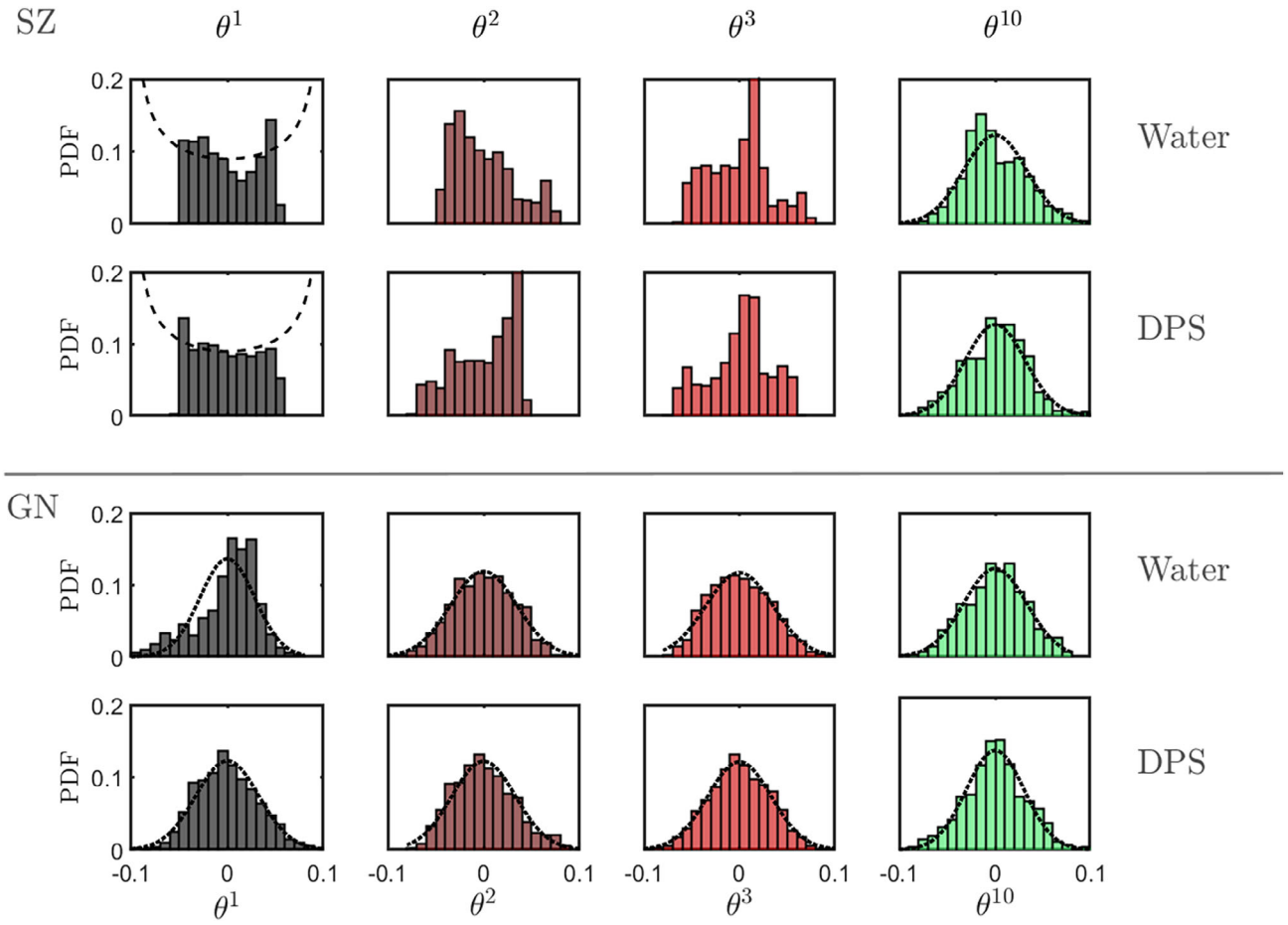


**FIGURE 6** Histogram plot of $\theta^i$ coefficient values (arbitrary units) for 1,000 instantaneous velocity fields. The same modes as Figure 5 are represented. Dotted lines and dashed lines are fittings of PDFs by respectively Gaussian functions (for apparently random modes) and Sinusoidal PDF trend (for apparently periodic modes). No trend lines are shown for modes with hybrid behavior ($\theta^2$ and $\theta^3$ in SZ) [Color figure can be viewed at wileyonlinelibrary.com]

power spectra approaches this −5/3 value is reduced, and pushed away to the high wave number range. For example, the $M_0 - end$ spectrum in DPS only roughly fits the theoretical slope in the $k \in [2.10^2, 6.10^2]$ $m^{-1}$ region while the fully reconstructed spectrum follows this trend in $k \in [6.10^1, 2.10^2]$ $m^{-1}$ as well.

Removing the first order modes from POD reconstruction in this case thus corresponds to artificially removing the largest scales of turbulence. This last remark leads to two conclusions. First, it is confirmed that in the FT region, no oscillatory motion is present or detectable by POD since the removal of low order modes immediately translates into a removal of large turbulent structures. Second, the importance of defining relevant criterion for the identification of oscillatory motion in grid stirred tank is further stressed out.

The simple use of a threshold mode number below which motion would be oscillatory and above which fluctuations would be turbulent is not a satisfactory solution. It can indeed, in some cases where oscillatory motion is weak, lead to a misrepresentation of turbulence properties.

## 4 | CONCLUSIONS

In water and DPS, most of the kinetic energy of the flow is contained in the first POD modes. This is especially true for regions of the flow close to or containing the grid's swept zone since in this region, the flow is governed by large coherent structures created by the grid's motion which are described by the first modes of the decomposition. The energetic dominance of the first modes is enhanced by the presence of polymer. The enhanced dominance of the first modes in DPS is a feature that cannot be only attributed to the forcing of the flow, but that is also significant in purely turbulent regions. It endorses the idea that the small structures of turbulence (here represented by the high mode numbers) are significantly damped in dilute polymer solutions as observed previously.[43] Whether this effect is here due to viscosity or to non-Newtonian properties is still open for discussion. The effect of polymer seems to be felt differently depending on the region: close to the grid it acts on the shape of organized motion, far from the grid on the structure of turbulence.

Criterion for the identification of organized motion in stirred tanks based on eigenvalue spectrum and temporal coefficient mostly fail to reveal oscillatory motion in OGT. This is not surprising in the FT region, since it is assumed that the intensity of oscillatory motion quickly decreases when moving away from the grid. Without identifying precisely the modes associated to oscillatory motion, defining an arbitrary cut-off mode number is obviously not fully satisfactory: removing the first POD modes leads to artificially remove kinetic energy from the reconstructed flow, and to a modification of the power spectra. Modes in the GN region shows only weak if any sign of oscillatory behavior. This is consistent with the fact that the periodic motion evidenced in phase resolved measurements was quite weak energetically compared to periodic motion in the SZ region.[40]

In this SZ region however, oscillatory motion is known to be strong. Even if two-mode coupling is not as clear as in stirred tanks, a different type of coupling involving at least three modes seems to appear. The exact reasons to why the link between mode coupling

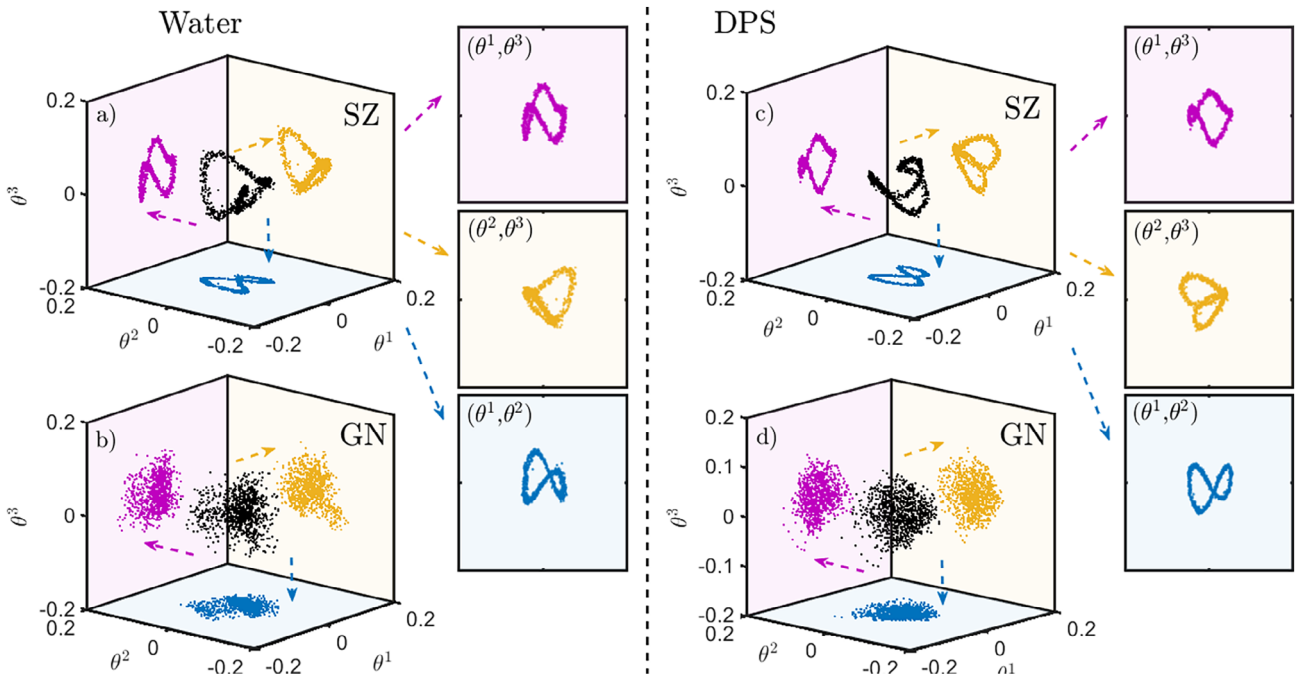


**FIGURE 7** Scatter plots of $(\theta_1,\theta_2,\theta_3)$ for water (a, b) and DPS (c, d) in the SZ (a, c) and GN (b, d) regions. 2D projections in planes $(\theta_1,\theta_2)$ (blue), $(\theta_2,\theta_3)$ (yellow), and $(\theta_1,\theta_3)$ (purple) are shown in figures a to d and extracted for sub-figures a) and c) [Color figure can be viewed at wileyonlinelibrary.com]

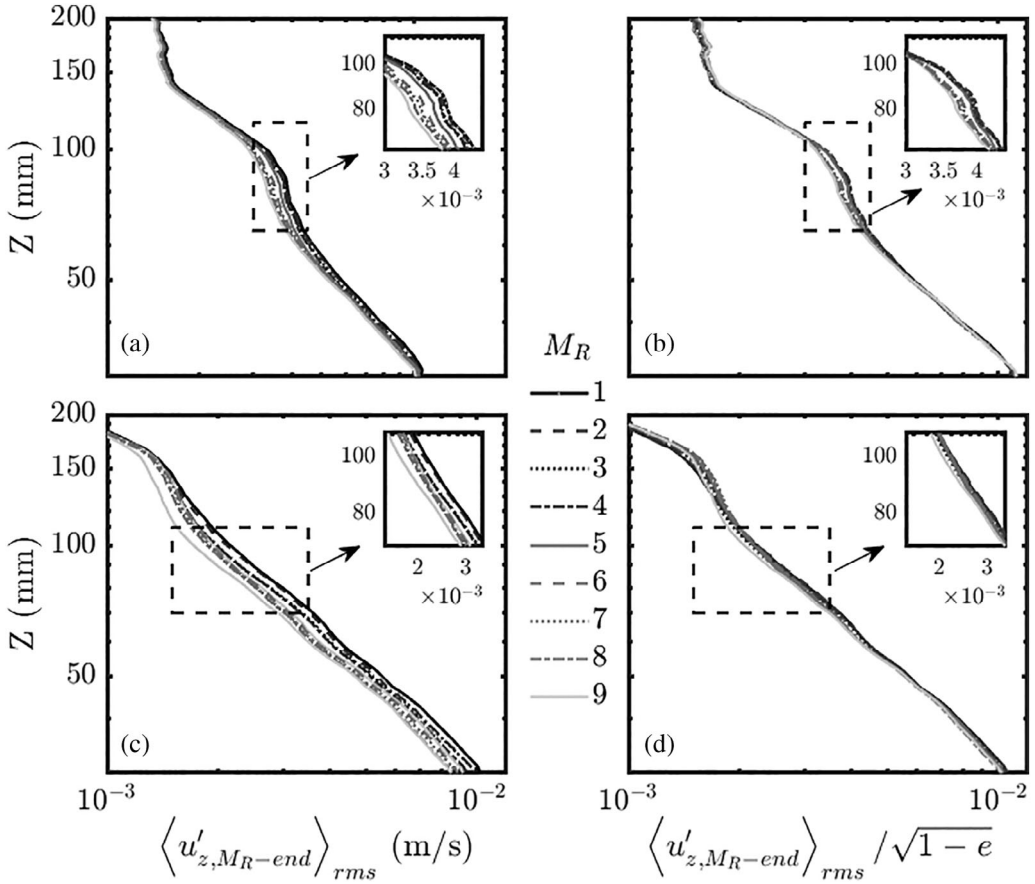


**FIGURE 8** Reconstructed rms profiles $\left\langle u'_{z,M_R-end} \right\rangle_{rms}$ for water (a, b) and DPS (c, d) after removal of the first $M_R$ modes, $M_R$ = 1 to $M_R$ = 9. (a) and (c) are reconstructed rms profiles, and (b) and (d) reconstructed profiles scaled to account for energy removal. Inserted sub-figures correspond to zooms on regions evidenced by dashed rectangle

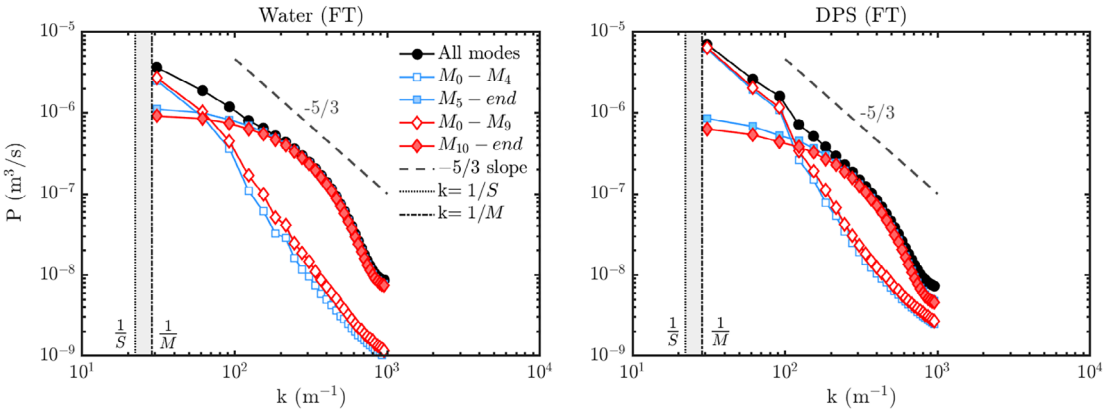


**FIGURE 9** POD reconstruction of turbulence total power spectrum $P = P_l + P_t$ using all the modes (black dots), modes 0 to 4 (empty blue squares), modes 5 and above (full blue squares), modes 0 to 9 (empty red diamonds), and modes 10 and above (full red diamonds). The grid energy input occurs at wave numbers between 1/*S* and 1/*M* (gray region). The expected inertial sub-range power law slope is also represented (dashed line) [Color figure can be viewed at wileyonlinelibrary.com]

and oscillatory motion seems more complex in the OGT situations than in stirred tank are yet to be understood. A first guess can be advanced: in POD studies applied to stirred tanks, the motion of the blade is always in the same direction. The oscillatory motion, that is to say vortex shedding by the blade, is thus always the same (same vortex propagation direction and rotation), and appears periodically. In the OGT case however, oscillatory eddies rotation is reversed whether the grid goes up or down. In the stirred tank case, turbulent

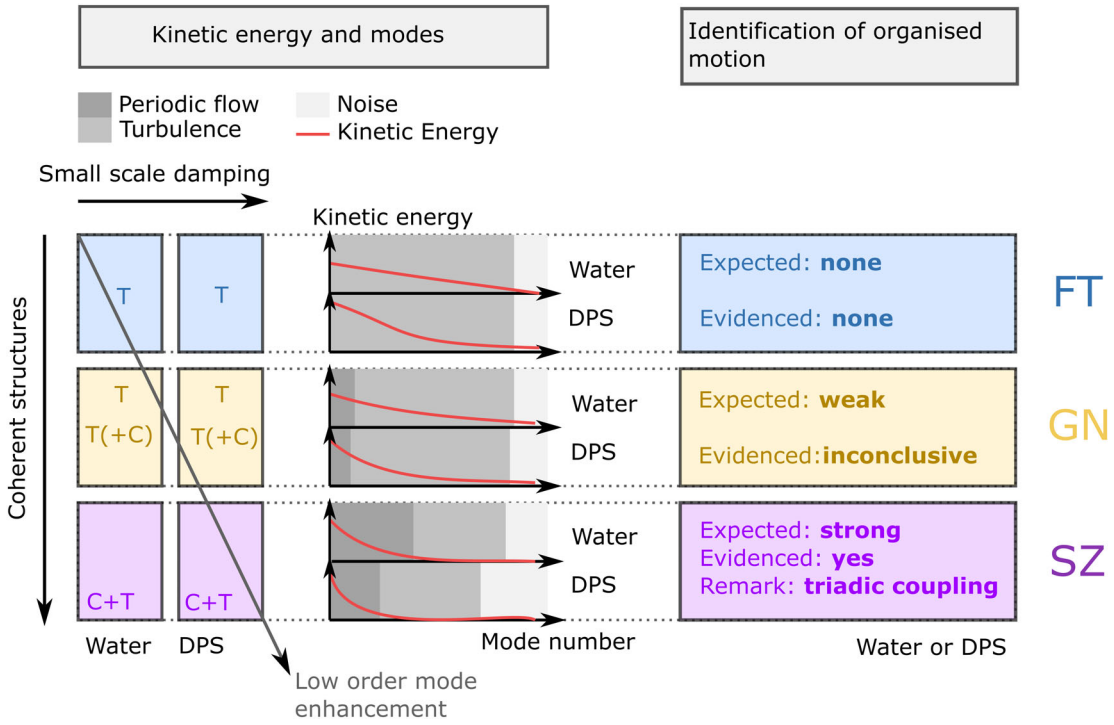


**FIGURE 10** Visual summary of the main conclusions of the present study regarding kinetic energy distribution in modes as a function of region of interest or fluid considered (left columns), and identification of organized motion (right column) [Color figure can be viewed at wileyonlinelibrary.com]

structures once generated by the blade evolve and dissipate freely in its wake. In the grid-stirred case on the other hand, eddies generated by one grid pass almost immediately re-interact with the grid half a period later. All the above strongly could make the model description more complex, likely to be associated with a (chaotic) near-grid mixing process efficient at low Reynolds numbers.

A visual summary of the previous conclusions is made in Figure 10.

It is well known that POD is useful to identify coherent fluid structures in various type of flows. In this work, we showed that the criterion for periodic flow identification may not always succeed. However POD still allows to isolate and remove flow features that are not purely intrinsic to turbulence from subsequent analysis, and avoid the pitfall of misinterpreting coherent fluctuations for turbulence. This is a first and crucial step towards proper modeling of turbulence properties in such flows.

Further investigations on the POD study of OGT should focus on this issue of oscillatory motion identification using modes. The structures observed on 3 modes temporal coefficient scatter plots suggest that a more complex mode coupling may exist, and so that criterion could be developed to identify periodic flows from POD decomposition in grid stirred tanks. This development of more universal criterion is of great interest for in the investigations of non-Newtonian effects on flow organization and oscillatory motion in grid stirred tanks, but also in more complex situations involving periodic forcing. Polymer concentration effect could then be investigated quite easily, even if a first simple approach using the tools of eigenvalue spectrum and Newtonian-normalized eigenvalue spectrum can also be considered (Figure 3). The use of a dynamic modes decomposition method (DMD,[49]) could also be considered as an interesting alternative to access additional information on temporal variation, despite the low temporal resolution of the data.

Finally, the similarities between the pattern observed in Figure 7 for the SZ region and the shape of chaotic attractors and associated trajectories raises an interesting question: the possible existence of an underlying chaotic process in oscillating grid flows that may be present in laminar cases and persist in turbulent cases, in the grid swept zone. Further works could be done in this sense.

## ACKNOWLEGEMENTS

The authors thank Dr. Gaby Launay, Dr. Neil Cagney and the two anonymous reviewers for their constructive remarks and feedback.

## ORCID

*Tom Lacassagne* https://orcid.org/0000-0003-3375-9921

## REFERENCES

1. Mcdougall TJ. Measurements of turbulence in a zero-mean-shear mixed layer. *J Fluid Mech*. 1979 Oct;94(03):409-431.
2. Chhabra RP, Richardson JF. *Non-Newtonian flow in the process industries: fundamentals and engineering applications*. Oxford,United Kingdom: Butterworth-Heinemann; 1999.
3. Kukura J, Arratia PC, Szalai ES, Bittorf KJ, Muzzio FJ. Understanding pharmaceutical flows. *Pharm Technol*. 2002;26(10):48-73.
4. Gabelle JC, Augier F, Carvalho A, Rousset R, Morchain J. Effect of tank size on kLa and mixing time in aerated stirred reactors with non-newtonian fluids. *Can J Chem Eng*. 2011;89(5):1139-1153.

5. Gabelle JC, Morchain J, Anne-Archard D, Augier F, Liné A. Experimental determination of the shear rate in a stirred tank with a non-newtonian fluid: Carbopol. *AIChE J*. 2013;59(6):2251-2266.
6. Chhabra RP. Non-Newtonian fluids: an Introduction. *Rheology of complex fluids*. New York, NY: Springer; 2010:3-34.
7. De Angelis E, Casciola CM, Benzi R, Piva R. Homogeneous isotropic turbulence in dilute polymers. *J Fluid Mech*. 2005;531:1-10.
8. Liberzon A, Guala M, Kinzelbach W, Tsinober A. On turbulent kinetic energy production and dissipation in dilute polymer solutions. *Phys Fluids*. 2006;18(12):125101.
9. Liberzon A. On the effects of dilute polymers on driven cavity turbulent flows. *Int J Heat Fluid Flow*. 2011;32(6):1129-1137.
10. Nguyen MQ, Delache A, Simoëns S, Bos WJT, EL Hajem M. Small scale dynamics of isotropic viscoelastic turbulence. *Phys Rev Fluids* 2016;1(8):083301.
11. Sreenivasan KR, White CM. The onset of drag reduction by dilute polymer additives, and the maximum drag reduction asymptote. *J Fluid Mech*. 2000;409:149-164.
12. Voulgaropoulos V, Zadrazil I, Brun NL, Bismarck A, Markides CN. On the link between experimentally-measured turbulence quantities and polymer-induced drag reduction in pipe flows. *AIChE J*. 2019;65(9): e16662.
13. Arratia PE, Kukura J, Lacombe J, Muzzio FJ. Mixing of shear-thinning fluids with yield stress in stirred tanks. *AIChE J*. 2006;52(7):2310-2322.
14. Rasschaert F, Talansier E, Blésès D, Magnin A, Lambert M. Packaging of yield stress fluids: flow patterns. *AIChE J*. 2018;64(3):1117-1126.
15. Liné A, Gabelle JC, Morchain J, Anne-Archard D, Augier F. On POD analysis of PIV measurements applied to mixing in a stirred vessel with a shear thinning fluid. *Chem Eng Res Des*. 2013 Nov;91(11): 2073-2083.
16. Variano EA, Cowen EA. Turbulent transport of a high-Schmidt-number scalar near an air-water interface. *J Fluid Mech*. 2013 Sep; 731:259-287.
17. Cocconi G, De Angelis E, Frohnapfel B, Baevsky M, Liberzon A. Small scale dynamics of a shearless turbulent/non-turbulent interface in dilute polymer solutions. *Phys Fluids*. 2017 Jul;29(7):075102.
18. Crawford AM, Mordant N, Xu H, Bodenschatz E. Fluid acceleration in the bulk of turbulent dilute polymer solutions. *New J Phys*. 2008;10 (12):123015.
19. Herlina H. Gas transfer at the air-water interface in a turbulent flow environment. (PhD thesis), Universitätsverlag Karlsruhe; 2005.
20. Hopfinger EJ, Toly JA. Spatially decaying turbulence and its relation to mixing across density interfaces. *J Fluid Mech*. 1976;78(01): 155-175.
21. Thompson SM, Turner JS. Mixing across an interface due to turbulence generated by an oscillating grid. *J Fluid Mech*. 1975;67(02): 349-368.
22. Voropayev SI, Fernando HJS. Propagation of grid turbulence in homogeneous fluids. *Phys Fluids*. 1996;8(9):2435-2440.
23. McCorquodale MW, Munro RJ. Experimental study of oscillating-grid turbulence interacting with a solid boundary. *J Fluid Mech*. 2017;813: 768-798.
24. McCorquodale MW, Munro RJ. Analysis of intercomponent energy transfer in the interaction of oscillating-grid turbulence with an impermeable boundary. *Phys Fluids*. 2018;30(1):015105.
25. Brumley BH, Jirka GH. Near-surface turbulence in a grid-stirred tank. *J Fluid Mech*. 1987;183:235-263.
26. Chiapponi L, Longo S, Tonelli M. Experimental study on oscillating grid turbulence and free surface fluctuation. *Experiments in Fluids*. 2012;53(5):1515-1531.
27. Lacassagne T, EL Hajem M, Morge F, Simoens S, Champagne JY. Study of gas liquid mass transfer in a grid stirred tank. *Oil Gas Sci Technol*. 2017;72(1):7.
28. McKenna SP, McGillis WR. The role of free-surface turbulence and surfactants in air-water gas transfer. *Int J Heat Mass Transf*. 2004;47 (3):539-553.
29. Verso L, van Reeuwijk M, Liberzon A. Steady state model and experiment for an oscillating grid turbulent two-layer stratified flow. *Phys Rev Fluids*. 2017;2(10):104605.
30. Xuequan E, Hopfinger EJ. On mixing across an interface in stably stratified fluid. *J Fluid Mech*. 1986;166:227-244.
31. Cuthbertson AJS, Samsami F, Dong P. Model studies for flocculation of sand-clay mixtures. *Coastal Eng*. 2018;132:13-32.
32. Mahamod MT, Mohtar WHMW, Yusoff SFM. Spatial and temporal behavior of Pb, cd and Zn release during short term low intensity resuspension events. *J Teknol*. 2017;80(1):17–25.
33. Nagami Y, Saito T. An experimental study of the modulation of the bubble motion by gas-liquid-phase interaction in oscillating-grid decaying turbulence. *Flow Turbul Combust*. 2013;92(1–2):147-174.
34. Rastello M, Michallet H, Marié JL. Sediment erosion in zero-mean-shear turbulence. *Coastal Dyn*. 2017;094:597-607.
35. San L, Long T, Liu CCK. Algal bioproductivity in turbulent water: an experimental study. *Water*. 2017;9(5):304.
36. Chu CR, Jirka GH. Turbulent gas flux measurements below the air-water interface of a grid-stirred tank. *Int J Heat Mass Transf*. 1992;35 (8):1957-1968.
37. Matsunaga N, Sugihara Y, Komatsu T, Masuda A. Quantitative properties of oscillating-grid turbulence in a homogeneous fluid. *Fluid Dyn Res*. 1999;25(3):147-165.
38. Nokes RI. On the entrainment rate across a density interface. *J Fluid Mech*. 1988;188:185-204.
39. Silva IPDD, Fernando HJS. Some aspects of mixing in a stratified turbulent patch. *J Fluid Mech*. 1992;240:601-625.
40. Lacassagne T, Lyon A, Simoëns S, Hajem ME, Champagne JY. Flow around an oscillating grid in water and shear-thinning polymer solution at low Reynolds number. *Exp Fluids*. 2019;61(1):15.
41. Liberzon A, Holzner M, Lüthi B, Guala M, Kinzelbach W. On turbulent entrainment and dissipation in dilute polymer solutions. *Phys Fluids*. 2009;21(3):035107.
42. Wang Y, Cai WH, Wei TZ, Wang L, Li FC. Experimental study on two-oscillating grid turbulence with polymer additives. Paper presented at: Fluids Engineering Division Summer Meeting, Seoul, South Korea: ASME; 2015. p. V001T15A008.
43. Wang Y, Cai WH, Wei TZ, Zhang HN, Wang L, Li FC. Proper orthogonal decomposition analysis for two-oscillating grid turbulence with viscoelastic fluids. *Adv Mech Eng*. 2016;8(11): 1687814016679773.
44. McComb WD, Allan J, Greated CA. Effect of polymer additives on the small-scale structure of grid-generated turbulence. *Phys Fluids*. 1977; 20(6):873-879.
45. Vonlanthen R, Monkewitz PA. Grid turbulence in dilute polymer solutions: PEO in water. *J Fluid Mech*. 2013;730:76-98.
46. Lacassagne T, Simoëns S, EL Hajem M, Lyon A, Champagne JY. Oscillating grid turbulence in shear-thinning polymer solutions. *Phys Fluids*. 2019;31(8):083102.
47. Escudié R, Liné A. Experimental analysis of hydrodynamics in a radially agitated tank. *AIChE J*. 2003;49(3):585-603.
48. Ducci A, Doulgerakis Z, Yianneskis M. Decomposition of flow structures in stirred reactors and implications for mixing enhancement. *Ind Eng Chem Res*. 2008;47(10):3664-3676.
49. de Lamotte A, Delafosse A, Calvo S, Toye D. Analysis of PIV measurements using modal decomposition techniques, POD and DMD, to study flow structures and their dynamics within a stirred-tank reactor. *Chem Eng Sci*. 2018;178:348-366.
50. Gabelle JC, Morchain J, Liné A. Kinetic energy transfer between first proper orthogonal decomposition modes in a mixing tank. *Chem Eng Technol*. 2017;40(5):927-937.

51. Graftieaux L, Michard M, Grosjean N. Combining PIV, POD and vortex identification algorithms for the study of unsteady turbulent swirling flows. *Meas Sci Technol*. 2001;12(9):1422-1429.
52. Hamdi J, Assoum H, Abed-Meraïm K, Sakout A. Volume reconstruction of an impinging jet obtained from stereoscopic-PIV data using POD. *Eur J Mech B*. 2018;67:433-445.
53. Lacassagne T. Oscillating grid turbulence and its influence on gas liquid mass trasnfer and mixing in non-Newtonian media. (PhD Thesis), University of Lyon; 2018.
54. Janzen JG, Herlina H, Jirka GH, Schulz HE, Gulliver JS. Estimation of mass transfer velocity based on measured turbulence parameters. *AIChE J*. 2010;56(8):2005-2017.
55. Wyatt NB, Liberatore MW. Rheology and viscosity scaling of the polyelectrolyte xanthan gum. *J Appl Polym Sci*. 2009;114(6):4076-4084.
56. Hussain AKMF, Reynolds WC. The mechanics of an organized wave in turbulent shear flow. *J Fluid Mech*. 1970;41(2):241-258.
57. Sirovich L. Turbulence and the dynamics of coherent structures. I. Coherent structures. *Q Appl Math*. 1987;45(3):561-571.
58. Moreau J, Liné A. Proper orthogonal decomposition for the study of hydrodynamics in a mixing tank. *AIChE J*. 2006;52(7):2651-2655.
59. Xie X, Dietrich N, Fillaudeau L, Le Men C, Schmitz P, Liné A. Local hydrodynamics investigation within a dynamic filtration unit under laminar flow. *Chem Eng Res Des*. 2018;132:954-965.
60. LaVision. DaVIs Flowmaster Manual. LaVision GmbH; 2011.
61. De Angelis E, Casciola CM, L'vov VS, Piva R, Procaccia I. Drag reduction by polymers in turbulent channel flows: energy redistribution between invariant empirical modes. *Phys Rev E*. 2003;67(5):056312.
62. Liné A. Eigenvalue spectrum versus energy density spectrum in a mixing tank. *Chem Eng Res Des*. 2016;108:13-22.
63. Ottino JM. Mixing, chaotic advection, and turbulence. *Annu Rev Fluid Mech*. 1990;22(1):207-254.
64. Pope SB. *Turbulent flows*. Cambridge, United Kingdom: Cambridge University Press; 2000.

## SUPPORTING INFORMATION

Additional supporting information may be found online in the Supporting Information section at the end of this article.

**How to cite this article:** Lacassagne T, Simoëns S, EL Hajem M, Champagne J-Y. POD analysis of oscillating grid turbulence in water and shear thinning polymer solution. *AIChE J*. 2021;67:e17044. https://doi.org/10.1002/aic.17044